Biochimie 128-129 (2016) 20–33

Contents lists available at ScienceDirect

Biochimie

journal homepage: www.elsevier.com/locate/biochi

Research paper

Structural comparison of AP endonucleases from the exonuclease III family reveals new amino acid residues in human AP endonuclease 1 that are involved in incision of damaged DNA

Modesto Redrejo-Rodríguez [a, 1, 2], Armelle Vigouroux [b, 1], Aibek Mursalimov [e, 1], Inga Grin [a, c, d, 1], Doria Alili [a], Zhanat Koshenov [e], Zhiger Akishev [f], Andrei Maksimenko [a], Amangeldy K. Bissenbaev [f], Bakhyt T. Matkarimov [e], Murat Saparbaev [a], Alexander A. Ishchenko [a, *], Solange Moréra [b, *]

[a] Laboratoire «Stabilité Génétique et Oncogenèse» CNRS, UMR 8200, Univ. Paris-Sud, Université Paris-Saclay, Gustave Roussy Cancer Campus, Equipe Labellisée Ligue Contre le Cancer, F-94805 Villejuif Cedex, France
[b] Institute for Integrative Biology of the Cell (I2BC), CNRS CEA Univ Paris-Sud, Université Paris-Saclay, Gif-sur-Yvette 91198, France
[c] SB RAS Institute of Chemical Biology and Fundamental Medicine, Novosibirsk 630090, Russia
[d] Department of Natural Sciences, Novosibirsk State University, Novosibirsk 630090, Russia
[e] National Laboratory Astana, Nazarbayev University, Astana 010000, Kazakhstan
[f] Department of Molecular Biology and Genetics, Faculty of Biology, Al-Farabi Kazakh National University, Almaty 530038, Kazakhstan

ARTICLE INFO

Article history:
Received 15 December 2015
Accepted 20 June 2016
Available online 22 June 2016

Keywords:
Oxidative DNA damage
Crystal structure
Base excision repair
Nucleotide incision repair
AP endonuclease

ABSTRACT

Oxidatively damaged DNA bases are substrates for two overlapping repair pathways: DNA glycosylase-initiated base excision repair (BER) and apurinic/apyrimidinic (AP) endonuclease-initiated nucleotide incision repair (NIR). In the BER pathway, an AP endonuclease cleaves DNA at AP sites and 3′-blocking moieties generated by DNA glycosylases, whereas in the NIR pathway, the same AP endonuclease incises DNA 5′ to an oxidized base. The majority of characterized AP endonucleases possess classic BER activities, and approximately a half of them can also have a NIR activity. At present, the molecular mechanism underlying DNA substrate specificity of AP endonucleases remains unclear mainly due to the absence of a published structure of the enzyme in complex with a damaged base. To identify critical residues involved in the NIR function, we performed biochemical and structural characterization of *Bacillus subtilis* AP endonuclease ExoA and compared its crystal structure with the structures of other AP endonucleases: *Escherichia coli* exonuclease III (Xth), human APE1, and archaeal Mth212. We found conserved amino acid residues in the NIR-specific enzymes APE1, Mth212, and ExoA. Four of these positions were studied by means of point mutations in APE1: we applied substitution with the corresponding residue found in NIR-deficient *E. coli* Xth (Y128H, N174Q, G231S, and T268D). The APE1-T268D mutant showed a drastically decreased NIR activity and an inverted Mg^{2+} dependence of the AP site cleavage activity, which is in line with the presence of an aspartic residue at the equivalent position among other known NIR-deficient AP endonucleases. Taken together, these data show that NIR is an evolutionarily conserved function in the Xth family of AP endonucleases.

Abbreviations: ROS, reactive oxygen species; AP, apurinic/apyrimidinic site; THF, tetrahydrofuran; αdN, alpha-anomeric 2′-deoxynucleosides; DHT, 5,6-dihydrothymine; DHU, 5,6-dihydrouracil; 5ohC, 5-hydroxycytosine; BER, base excision repair; NIR, nucleotide incision repair; APE1, human AP endonuclease 1; ExoIII, *Escherichia coli* exonuclease III; Nfo, *Escherichia coli* endonuclease IV; ExoA, *Bacillus subtilis* exonuclease III; BsNfo, *Bacillus subtilis* endonuclease IV.

* Corresponding authors.
E-mail addresses: alexander.ishchenko@gustaveroussy.fr (A.A. Ishchenko), solange.morera@i2bc.paris-saclay.fr (S. Moréra).

[1] These authors contributed equally.

[2] Present Address: Centro de Biología Molecular “Severo Ochoa”, Consejo Superior de Investigaciones Científicas and Universidad Autónoma de Madrid, 28049 Madrid, Spain.

http://dx.doi.org/10.1016/j.biochi.2016.06.011

1. Introduction

Aerobic respiration gives rise to production of reactive oxygen species (ROS), which damage cellular macromolecules. DNA is prone to spontaneous decomposition and is a primary target of ROS, which produce an array of oxidative modifications of the base and sugar backbone [1,2]. In the absence of repair and cell renewal, spontaneous and oxidative types of DNA damage tend to accumulate and may lead to premature aging, cancer, and neurodegenerative diseases [3]. The majority of oxidatively damaged DNA bases including 5,6-dihydrothymine (DHT), 5,6-dihydrouracil (DHU), 5′-hydroxyuracil (5ohU), 5-hydroxycytosine (5ohC), and pyrimidine-derived hydantoins are substrates for two overlapping pathways: DNA glycosylase-initiated base excision repair (BER) and AP endonuclease-mediated nucleotide incision repair (NIR) [4–6]. At the first step of the BER pathway, a DNA glycosylase hydrolyses the N-glycosidic bond between the damaged base and the sugar, leaving either an apurinic/apyrimidinic (AP) site or a single-stranded DNA break [7]. At the second step, an AP endonuclease cleaves 5′ next to the AP site leaving a single-stranded DNA break flanked with a 3′-hydroxyl group (3′-OH) and a 5′-deoxyribose phosphate moiety, or removes 3′-blocking groups in the one-nucleotide (nt) gap to generate clean 3′-OH termini. Alternatively, in the NIR pathway, an AP endonuclease directly cleaves 5′ next to a damaged base and generates a single-strand break flanked with a 5′ dangling modified nucleotide and 3′-OH terminus [8]. Despite the general assumption that BER, initiated by multiple DNA glycosylases, is the main pathway for removal of the majority of oxidized bases [9], certain types of lesions such as the α-anomers of 2′-deoxynucleosides (αdA, αdC, and αT) are not repaired by DNA glycosylases but rather by AP endonucleases in the NIR pathway [10,11]. In line with this observation, we demonstrated that expression of the NIR-deficient *Escherichia coli* endonuclease IV (Nfo) mutants in an AP endonuclease-null strain of *E. coli* suppresses its hypersensitivity to alkylation but not to oxidative DNA damage, suggesting that the NIR pathway is necessary for protection of cells from potentially lethal oxidative DNA lesions [12]. The NIR pathway can be found in all three domains of life—Archaea, Bacteria, and Eukaryota—with the well characterized AP endonucleases of *Methanothermobacter thermautotrophicus* ΔH Mth212, *E. coli* endonuclease IV, and human APE1 proteins [6,8,13].

AP endonucleases are multifunctional DNA repair enzymes. In addition to their main activity (AP site cleavage), they can also show 3′-repair phosphodiesterase, 3′→5′ exonuclease, and/or NIR activities, albeit at lower efficiency [14–16]. Moreover, all of these DNA repair functions are catalyzed by the single active site [17,18]. AP endonucleases are subdivided into two distinct families based on structural folding and amino acid sequence similarity to either *Escherichia coli* exonuclease III (Xth, Mg^{2+}-dependent) or endonuclease IV (Nfo, independent of external divalent cations) [19]. Structural studies reveal that Xth and Nfo families of AP endonucleases have two distinct highly conserved three-dimensional folds: the Xth fold contains a two-layered β-sheet core flanked by helices, whereas the Nfo fold contains a TIM β-barrel core, surrounded by helices [17]. Although Xth and Nfo AP endonuclease families have overlapping DNA substrate specificity, they are distinguished by their modes of DNA damage recognition. Indeed, cocrystal structures of Nfo bound to an AP site analog, tetrahydrofuran, revealed that the DNA helix is drastically distorted by ~90° bending with flipping out not only of the target AP site of the DNA base stack but also of its opposing nucleotide [20,21]. In contrast, cocrystal structures of human APE1, which belongs to the exonuclease III family, bound to abasic-site-containing DNA showed that the DNA helix is kinked by only 35° with an AP site flipped out into the active site pocket that excludes DNA bases, while the opposite base remains stacked in the duplex [22]. Furthermore, all APE1-catalyzed DNA repair activities require the presence of divalent metal ions. Moreover, the DNA substrate specificity of the human enzyme varies dramatically depending on cation concentration [6,23,24]. Indeed, divalent metal ions, pH, and ionic strength requirements of the APE1-catalyzed AP endonuclease activity *versus* NIR activity are drastically different: NIR activity requires low concentrations of Mg^{2+} (≤1 mM) and acidic/neutral pH (≤7), whereas maximal AP site cleavage activity is achieved at high concentrations of Mg^{2+} (≥5 mM) and pH values between 6.6 and 8.6 [25,26]. The 3′-repair phosphodiesterase activity of APE1 requires the same reaction conditions as AP site cleavage activity. Nevertheless, maximal activity can be achieved at low Mg^{2+} concentrations (1–2 mM) [23].

Contrary to APE1 and Mth212, previously reported prokaryotic exonuclease III family AP endonucleases lack a NIR function, e.g., *E. coli* Xth and *Mycobacterium tuberculosis* exonuclease III (MtbXthA) [8,27]. These observations raise the question about the evolutionary process that leads to a loss or gain of new DNA repair function. In the present study, to further explore the molecular basis of the NIR function, we analyzed another member of the Xth group: ExoA from the gram-positive bacterium *Bacillus subtilis.* Just as in *E. coli* and other bacteria, the genome of *B. subtilis* encodes two AP endonucleases: BsNfo (originally referred to as YqfS and encoded by the *yqfS* gene) and ExoA (encoded by the *exoAA* gene), both important for protection of germinating spores (for cell growth) from abasic sites and from strand breaks in DNA induced by endogenous and exogenous factors [28]. Genetic studies have revealed that the lack of ExoA, or both ExoA and BsNfo, sensitizes spores to dry-heat treatment but not to wet heat and genotoxic agents, including N-methyl-N′-nitro-N-nitrosoguanidine (MNNG), H_2O_2, and *tert*-butyl hydroperoxide (*t*-BuO_2H) [29,30]. Nevertheless, outgrowing spores lacking both ExoA and BsNfo are sensitive to H_2O_2 and show increased mutation rates suggesting that these AP endonucleases contribute to repair of DNA damage during vegetative growth of *B. subtilis* [28,31]. The enzymatic activity of recombinant ExoA has been previously characterized: ExoA is a multifunctional AP endonuclease [29]. However, the possible presence of the NIR function in *Bacillus* AP endonucleases has not been studied. Here, we have analyzed the DNA substrate specificity of ExoA in more detail including its NIR activity and we determined its crystal structure at 1.84 Å resolution. According to the structural comparison of *B. subtilis* ExoA with *E. coli* Xth (PDB code 1AKO), human APE1 (PDB code 1DEW), and with archaeal Mth212 (PDB code 3G00), four single amino acid residues in APE1 were substituted with homologous ones identified in Xth. The resulting APE1 mutants were characterized for their DNA substrate specificity. Strikingly, we found that substitution of T268 (an amino acid residue located outside the active site, and involved in DNA contact) had a dramatic effect on the NIR function and Mg^{2+} dependence. The evolutionary selection of this residue as a possible hallmark of NIR capacity is discussed.

2. Materials and methods

2.1. Reagents and oligonucleotides

All oligodeoxyribonucleotides containing modified residues, and their complementary oligonucleotides were purchased from Eurogentec (Seraing, Belgium), including the following: 30 mer for kinetic studies d(TGACTGCATAXGCATGTAGACGATGTGCAT) where X is either alpha-anomeric 2'-deoxyadenosine (αdA), 5,6-dihydrouracil (DHU), 5,6-dihydrotymine (DHT), 5-hydroxycytosine (5ohC), 5-methylcytosine (5 mC), 5-hydroxymethylcytosine (5ohmC), 1,N^6-ethenoadenine (εA), uracil

(U), urea, 5*R*-6*S*-thymine glycol (Tg), 7,8-dihydro-8-oxoguanine (8oxoG) or tetrahydrofuranyl (THF), and 30 mer complementary oligonucleotide, containing either dA, dG, dC or T opposite the adduct. Oligonucleotides were either 5'-end labeled by T4 polynucleotide kinase (New England Biolabs, OZYME France) in the presence of [γ-^{32}P]-ATP (3000 Ci·mmol^{-1}) (PerkinElmer SAS, France), or 3'-end labeled by terminal transferase (New England Biolabs) in the presence of [α-^{32}P]-3'-dATP (Cordycepin 5'-triphosphate, 5000 Ci·mmol^{-1}) (PerkinElmer) as recommended by the manufacturers. It should be noted that after [^{32}P]-3'-dAMP labeling of 30 mer oligonucleotides, their lengths extended by one nucleotide. Oligonucleotides were annealed as previously described [32]. The resulting duplex oligonucleotides are referred to as X·N, where X is a modified residue and N is an opposite residue (C, G, A or T) in complementary strand, respectively.

The following oligonucleotides were used to measure 3'→5′ exonuclease and 3'-repair diesterase activities: Exo20, d(GTGGCGCGGAGACTTAGAGA); Exo20^{THF}, d(GTGGCGCGGAGACTTAGAGAX), where X is 3'-terminal THF; Exo20^{P}, d(GTGGCGCGGAGACTTAGAGAp), where p is 3'-terminal phosphate; 5P-Exo19, d(pATTTGGCGCGGGGAATTCC), where p is 5'-terminal phosphate; and complementary Rex-T, d(GGAATTCCCCGCGCCAAATTTCTCTAAGTCTCCGCGCCAC). The nicked/gapped duplexes, Exo20·T, Exo20^{THF}·T, Exo20^{P}·T were comprised of 5P-Exo19 and Rex-T, and Exo20, or Exo20^{P}, or Exo20^{THF}, respectively. Schematic representations of the oligonucleotide duplexes used in the present work can be found in Fig. S1.

In the present study, to measure the 3'-phosphatase activity of the AP endonucleases, we prepared 20 mer (Exo20) oligonucleotide containing 3'-terminal radioactive phosphate residue - ^{32}P. Previously, we have shown that human tyrosyl-DNA phosphodiesterase 1 (Tdp1) can remove 3'-terminal cordycepin nucleoside producing an oligonucleotide fragment with a phosphate residue at the 3′ end [33]. For this, Exo20 was 3'-end labeled using cordycepin [α-^{32}P]-3'-dATP to obtain a 21 mer Exo20-[^{32}P]-3'-dAMP fragment, which was then treated with recombinant Tdp1 (generously provided by Prof. Olga Lavrik, Novosibirsk, Russia). The resulting 20 mer Exo20-3′-^{32}P fragment and 5P-Exo19 oligonucleotide were annealed to the complementary Rex-T oligonucleotide and the resulting Exo20^{P}·T gapped duplex oligonucleotide was used as the DNA substrate to measure the 3'-phosphatase activity of AP endonucleases under steady state reaction conditions.

2.2. *E. coli* strains and plasmids

Escherichia coli strain BH110 (*nfo::kan^{R} [Δ(xthA-pncA)90 X::Tn10]*), is an isogenic derivative of AB1157, was from the laboratory stock [32]. *B. subtilis* ExoA was PCR-amplified from genomic DNA provided by Dr. U. Mechold (Institut Pasteur, Paris, France) with oligonucleotide primers d(GGATCCATGAAGTTGATTTCATGGAA) and d(CATATGTCATATATTGATGATAAGTT).

The native non-tagged wild-type (WT) and mutant human APE1 proteins were expressed and purified using AP endonuclease deficient *E. coli* strain and expression vector pET11a-APE1 as described previously [34]. Site-directed mutations within the APE1 coding sequence in pET11a-APE1 were generated using the QuickChange site-directed mutagenesis kit (Quickchange® XL, Site-Directed Mutagenesis Kit, Stratagene). The strain BH110 was lysogenized with the helper phage (λDE3) harboring a copy of the T7 RNA polymerase gene, using the DE3 lysogenization kit (Novagen, Merck4Biosciences, France). The resulting *E. coli* BH110 (DE3) was transformed by pET vectors encoding ExoA and APE1 under control of the T7 promoter.

2.3. Purification procedure

The purified *E. coli* endonuclease VIII (Nei) and AP endonuclease Nfo were from the laboratory stock. The non-tagged native human APE1 wild type and mutant proteins were expressed and purified from *E. coli* BH110 (DE3) strain to avoid cross contamination with bacterial AP endonucleases as described elsewhere [4].

Bacillus subtilis ExoA was purified from *E. coli* BH110(DE3) strain, transformed by electroporation with pET11a-ExoA plasmid. For protein overexpression and purification, overnight saturated cultures were diluted 1:100 in fresh LB and grown to OD_{600nm} = 0.6–0.7 at 30 °C. Then, protein was induced by 0.1 mM isopropyl β-D-1-thiogalactopyranoside (IPTG) overnight at room temperature. Cells were harvested by centrifugation and resuspended in 1/50 vol of lysis buffer (20 mM Hepes-KOH pH 7.6, 40 mM NaCl) supplemented with Complete™ Protease Inhibitor Cocktail (Roche, Switzerland) and a lysed with a French press at 18,000 psi. The homogenate was centrifuged at 40,000*g* for 30 min (4 °C) and the supernatant was passed through a column packed with 50 mL of Q-Sepharose Fast Flow resin (GE Healthcare) pre-equilibrated in the same buffer. The flow-through fractions containing ExoA were pooled and loaded onto a 1 mL HiTrap-Heparin^{tm} column (GE Healthcare). Bound proteins were eluted in a 20–600 mM KCl gradient. The purified protein samples were pooled and buffer-exchanged with a PD-10 Desalting column (GE Healthcare) pre-equilibrated in 20 mM Hepes-KOH pH 7.6, 50 mM NaCl. When required, purified protein was concentred with a Microcon centrifugal filter unit YM10 (Merk-Millipore).

2.4. DNA repair assays

The standard incision assay conditions (20 μL) contained 5 nM [^{32}P]-labeled of each duplex oligonucleotide substrate and the indicated amount of enzyme in an optimized enzyme-specific buffer. Thus, the reference reaction buffer contained 50 mM KCl, 20 mM HEPES-KOH pH 7.6, 0.1 mg mL^{-1} BSA and 1 mM DTT. *B. subtilis* ExoA reactions were complemented with 1 mM $MgCl_2$, except otherwise stated, whereas control reactions with *E. coli* Nei and Xth proteins were performed in the standard reaction buffer supplemented with KCl up to 100 mM, and with 1 mM EDTA or 5 mM $CaCl_2$, respectively. Human APE1 assay conditions vary depending on the DNA repair pathways studied. The standard AP endonuclease assay was performed under high Mg^{2+} concentration (≥5 mM) and pH 7.6 (BER conditions): the reaction mixture (20 μL) contained 5 nM [^{32}P]-labeled THF·T duplex oligonucleotide, 5 mM $MgCl_2$, 100 mM KCl, 20 mM Hepes-KOH pH 7.6, 0.1 mg mL^{-1} BSA and 10 pM of the enzyme, unless specified otherwise. The standard NIR assay was performed at a low Mg^{2+} concentration (≤1 mM) and acidic/neutral pH (≤7) (NIR conditions): the reaction mixture (20 μL) contained 5 nM [^{32}P]-labeled αdA·T or other DNA base lesions-containing duplex oligonucleotide, 0.5 mM $MgCl_2$, 50 mM KCl, 20 mM Hepes-KOH pH 6.8, 0.1 mg mL^{-1} BSA and 0.2 nM APE1, unless specified otherwise. The standard exonuclease and 3'-repair diesterase assays were also performed at low Mg^{2+} concentrations (≤1 mM) and acidic/neutral pH (≤7): the reaction mixture (20 μL) for APE1 protein contained 5 nM [^{32}P]-labeled Exo20·G, or Exo20^{THF}·T, or Exo20^{P}·T nicked/gapped duplex oligonucleotide, 1 mM $MgCl_2$, 50 mM KCl, 20 mM Hepes-KOH pH 6.8, 0.1 mg mL^{-1} BSA, and 0.2 nM of the enzyme, unless specified otherwise. All assays were performed at 37 °C for 10 min, unless specified otherwise. Reactions were stopped by adding 10 μL of a solution containing 0.5% SDS and 20 mM EDTA and then desalted in hand-made spin-down columns filled with Sephadex G25 (GE Healthcare) equilibrated in 7 M urea, unless otherwise stated. It should be noted that the samples were not desalted when analyzing the

products of reaction generated by the 3'-phosphatase and 3'→5′ exonuclease activities of AP endonucleases, unless otherwise stated. In these cases, the reactions were stopped by adding 10 μL of a solution containing 0.5% SDS, 20 mM EDTA and 7 M Urea. Finally, the purified and non-purified reaction products were heated at 95 °C for 3 min and then separated by electrophoresis on denaturing 20% (w/v) polyacrylamide gels (7 M urea, 0.5 × TBE). The gels were exposed to a Fuji FLA-3000 Phosphor Screen, then scanned with Fuji FLA-3000 or FLA-9500, and analyzed using Image Gauge V4.0 software. Unless otherwise specified, all enzymatic assays were repeated at least three times.

To measure kinetics parameters, 0.1–100 nM (or up to 5 μM for DHU·G) of duplex oligonucleotide substrate was incubated under standard reaction conditions. For K_M and k_{cat} determination, the linear velocity was measured and the constants were determined from Lineweaver-Burk plots. The kinetic parameters for exonuclease activity, when multiple degradation fragments appeared, were determined by measuring the reaction products as integrated intensities of the fragments (expressed as percentage of total substrate). The value obtained for each fragment was multiplied by the number of catalytic events required for its formation, and total exonuclease degradation was calculated as the sum of those products.

2.5. Crystallization, data collection and processing of ExoA and APE1

Crystallization trials for ExoA at 17 mg mL^{-1} were screened in sitting-drop vapour-diffusion experiments using the Classics suites and PEG II suites from Quiagen on a nanodrop robot (Cartesian, Proteomic Solution). Condition 40 from PEG II suites was manually optimized at 293 K with home made solution in hanging drops composed of a 1:1 vol ratio of crystallization solution (16% PEG 4000, 0.1 M Tris pH 8.5, 0.2 M $CaCl_2$). Crystallization trials for wild-type and D210 N APE1 at 20 mg mL^{-1} in presence of a damaged DNA 15-mer (αdA·T or DHU·T) in a molarity ratio 1:1 or 1:5 respectively were also screened. Conditions F8 (20% PEG 8000, 200 mM MgAc and 100 mM cacodylate pH 6.6) and B1 (70% MPD and 100 mM Hepes-KOH pH 7.5) from PEG II suites led to crystals. Crystals were flash-frozen in a cryo-protectant solution (mother solution supplemented with 22% or 25% PEG 400 for PEG condition) or directly for MPD conditions.

Data-collection experiments were carried out at 100 K on the PROXIMA 1 beamline at SOLEIL synchrotron (Saint Aubin, France) for ExoA crystals and on PROXIMA 2 beamline for APE1 crystals. Diffraction intensities were integrated with the program XDS [35]. Structure determination was performed by molecular replacement with PHASER [36] using the coordinates of human APE1 (PDB code 1BIX [37]), as a search model. Co-crystals of APE1-DNA were finally DNA-free APE1 from two crystals forms (form I corresponding to PDB code 1BIX and form II corresponding to 4LND). Refinement was performed with BUSTER-2.10 [38]. Electron density map was evaluated using COOT [39]. Molecular graphics images were generated using PYMOL (http://www.pymol.org). Data collection and processing statistics are given Table 1.

Table 1
Crystallographic data.

Protein/PDB code	ExoA/5CFE	APE1/5CFG
Space group Cell parameters (Å,°)	$P2_12_12_1$ $a = 52.3$ $b = 61.9$ $c = 73.3$	C2 a = 86.5 b = 45.1 c = 78 $\beta = 105.1$
Resolution (Å)	45–1.84 (1.95–1.84)	45–1.8 (1.9–1.8)
No. of observed reflections	124,963 (19,843)	98,262 (15,351)
No. of unique reflections	21,096 (3324)	27,028 (4259)
R_{sym} (%)	11.4 (66.2)	10.3 (73.2)
Completeness (%)	99.6 (99.1)	99.3 (98)
I/σ	12.1 (3)	9.1 (2)
R_{cryst} (%)	16.7	18.5
R_{free} (%)	20.7	20.4
rms bond deviation (Å)	0.009	0.01
rms angle deviation (°)	1.07	1.07
Average B ($Å^2$)		
protein	20.9	29.2
ligand	16.9	32
solvent	24.6	33.6

3. Results

3.1. Bacillus subtilis ExoA cleaves oligonucleotide duplexes containing a synthetic AP site and αdA

Other studies revealed that exonuclease III family AP endonucleases from *E. coli* (Xth), humans (APE1), and possibly *B. subtilis* (ExoA) have an absolute requirement for divalent cations, typically Mg^{2+}, for their catalytic activities [25,29,40]. We thus measured the DNA cleavage activity of ExoA on THF·T and αdA·T duplexes under reaction conditions optimal for Xth and APE1. For this purpose, we used 3′-end [^{32}P]3′-dAMP-labeled duplexes as DNA substrates in order to determine the mechanism of action of enzymes and to discriminate between of a bifunctional AP lyase/DNA glycosylase activity and an NIR-AP endonuclease activity [8]. A NIR-AP endonuclease cleaved 5′ next to damaged base and generated two cleavage fragments: the 5′ upstream fragment with a 3′-OH group and a 3′ downstream cleavage fragment containing a 5′-damaged dangling nucleotide. In contrast, a bifunctional AP lyase/DNA glycosylase excised the damaged base and then cleaved DNA 3′ next to the remaining AP site thus generating a 5′ upstream fragment with a 3′ blocking sugar phosphate group and a 3′ downstream cleavage fragment with 5′-terminal phosphate. Consequently, the size of 3′-cleavage fragments differed by one nucleotide between the NIR and BER pathways, and this difference could be detected by denaturing PAGE only if the DNA substrate was labeled at the 3′-end. As shown in Fig. 1A, a control treatment of 3′-end [^{32}P]-3′-dAMP-labeled duplexes by APE1 generated a 21-mer cleavage product that migrated faster than the 31-mer substrate. Incubation of THF·T and αdA·T substrates with ExoA yielded the same cleavage products as APE1 did (lanes 3–12), suggesting that ExoA has both AP endonuclease and NIR activities. After an increase in protein concentration, ExoA showed a nonspecific 3′→5′ exonuclease activity on both DNA duplexes that led to the gradual disappearance of both the 3′-end labeled DNA substrates and cleavage products in the gel (lanes 5–12). Nevertheless, in agreement with another study [29], ExoA cleaved a synthetic AP site with high efficiency, at enzyme concentrations of 0.1 and 0.5 nM, depending on Mg^{2+} concentration. ExoA could cleave 50% and 100% of 100 nM THF·T duplex in 10 min (lanes 4 and 5). To measure ExoA-catalyzed cleavage of the αdA·T duplex, only 10 nM ExoA and low $MgCl_2$ concentrations were used, in order to limit the nonspecific exonuclease activity of the enzyme. We observed cleavage of the αdA·T duplex next to the αdA site in the absence and presence of 0.1 mM $MgCl_2$ (lanes 11–12). Nevertheless, the NIR activity of ExoA under experimental conditions used here was much lower as compared to its AP endonuclease activity on the THF·T duplex.

To determine whether the apparent loss of the DNA substrates and products during incubation with ExoA (Fig. 1A) is due to the nonspecific 3′→5′ exonuclease activity of the bacterial enzyme, we analyzed the reaction products without desalting the samples. For this purpose, 3′-end [^{32}P]labeled THF·T and αdA·T duplexes were incubated with human APE1 or *B. subtilis* ExoA proteins, and after

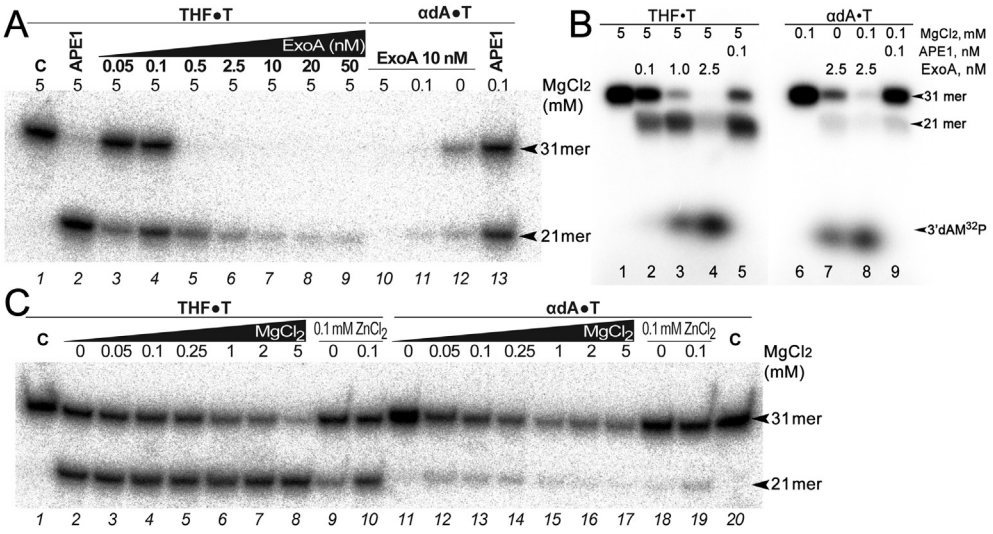

Fig. 1. Incision action of *B. subtilis* ExoA on 3′-end [^{32}P]-3′-dAMP-labeled THF·T and αdA·T oligonucleotide duplexes. (**A**) PAGE analysis of incision assays of THF·T (lanes 1–9) and αdA·T substrates (lanes 10–13). AP endonuclease was evaluated with a THF·T substrate incubated either with APE1 (0.5 nM, lane 2) or with increasing concentrations of ExoA (0.05–50 nM, lanes 3–9) in a buffer containing 5 mM $MgCl_2$. The NIR substrate αdA·T was treated with 10 nM ExoA in the presence of 5, 0.1, or 0 mM $MgCl_2$ (lanes 10–12) and APE1 under NIR conditions (lane 13). (**B**) Analysis of the reaction products in undesalted samples on short running time denaturing PAGE. THF·T (lanes 1–5) and αdA·T (lanes 6–9) substrates were incubated or not incubated with APE1 and varied amounts of ExoA in the presence of 5 mM and 0.1 mM $MgCl_2$, respectively. (**C**) Metal dependence of ExoA (0.25 nM) incision on THF·T (lanes 2–8) and αdA·T (lanes 11–17) substrates in the presence of the indicated concentration of $MgCl_2$ and/or $ZnCl_2$. Substrate and incision product sizes are indicated on the left. "**c**" indicates control reactions without an enzyme. For details see Materials and Methods.

the reaction, the samples were directly loaded and shortly analyzed by a denaturing PAGE without chromatographic desalting in order to visualize all the reaction products. As shown in Fig. 1B, under these reaction conditions, APE1 cleaved 3′-[^{32}P]labeled THF·T and αdA·T duplexes and generated 21-mer cleavage fragments but not radiolabeled dAMP residues (lanes 5 and 9). ExoA also cleaved the 3′-[^{32}P]labeled duplexes and produced 21-mer cleavage fragments, but in addition, it generated fast-running radiolabeled dAMP residues (lanes 3–4 and 7–8), indicating the presence of a 3′→5′ exonuclease activity that removes the 3′-terminal [^{32}P]-3′-dAMP nucleotide in a nonspecific manner. Moreover, when we used a 10-fold lower amount of the protein (0.1 nM), ExoA cleaved the 3′-[^{32}P] labeled THF·T duplex without generating a significant amount of the radiolabeled dAMP residues (lane 2). These results indicate that the loss of radiolabeled material during incubation with the bacterial AP endonuclease is due to its nonspecific 3′→5′ exonuclease activity.

Next, we examined in detail the dependence of ExoA-catalyzed DNA repair activities on divalent metal concentration. As shown in Fig. 1C, in the presence of a limiting concentration of the enzyme (0.25 nM), ExoA cleaved THF·T without a divalent cation, and its AP endonuclease activity increased with the increase in Mg^{2+} concentration, reaching a maximum of cleavage at 5 mM $MgCl_2$, within the range of concentrations of $MgCl_2$ tested (lanes 2–8). The presence of 0.1 mM $ZnCl_2$ in reaction buffer inhibited AP endonuclease activity of ExoA (lane 9) as compared to the buffer without divalent cations (lane 2), but addition of 0.1 mM Mg^{2+} restored the cleavage activity of ExoA (lane 10). ExoA cleaved the αdA·T duplex with low efficiency (only 20% substrate cleavage at 0.05 mM $MgCl_2$), and this activity was not stimulated by higher $MgCl_2$ concentrations as compared to AP site cleavage activity (lanes 12–17). Under these conditions, no significant cleavage of the αdA·T duplex was observed in the absence of Mg^{2+}, whereas addition of 0.1 mM $ZnCl_2$ inhibited 3′→5′ exonuclease but not NIR activity of ExoA (lane 19 *versus* 13). Taken together, these data suggest that ExoA is a metal-dependent enzyme endowed with a weak NIR activity and a highly efficient AP site cleavage activity.

3.2. Characterization of DNA substrate specificity of *B. subtilis* ExoA using oligonucleotide duplexes containing various modified DNA bases

We further examined the DNA substrate specificity of ExoA by means of oligonucleotide duplexes containing various DNA base modifications, including urea, thymine glycol (Tg), 5,6-dihydrothymine (DHT), 5,6-dihydrouracil (DHU), 5-hydroxycytosine (5ohC), 8-oxo-7,8-dihydroguanine (8oxoG), 1,N^6-ethenoadenine (εA), uracil (U), 5-methylcytosine (5 mC), and 5-hydroxymethylcytosine (5ohmC). As a control and also to generate the DNA size markers, we incubated the DHU·G duplex with *E. coli* DNA glycosylase Nei, *E. coli* Nfo, and human APE1. The 3′-end-labeled duplexes were incubated with ExoA or control repair enzymes, and the reaction products were analyzed by denaturing PAGE in a 20% gel.

As shown in Fig. 2, control NIR AP endonucleases Nfo and APE1 generated [^{32}P]labeled 21-mer cleavage fragments (lanes 3–4), which migrated more slowly than did the 20-mer products generated by DNA glycosylase Nei (lane 2). This cleavage pattern indicated that Nfo and APE1 incised 5′ next to a damaged nucleotide and generated a 21-mer cleavage product containing a 5′-dangling DHU nucleotide (lanes 3–4), whereas Nei excised the DHU base and cleaved the remaining AP site on the 3′ side, thus generating a 20-mer cleavage product that lacks the damaged nucleotide (lane 2). The results revealed that in addition to THF·T and αdA·T duplexes, ExoA also cleaves Urea·T, DHU·G, DHT·A, and 5ohC·G (Fig. 2, lanes 6, 8–10, and 14 and Fig. S2). Furthermore, the cleavage fragments generated by ExoA migrated at the same position in the electrophoretic gel as did the products of NIR AP endonucleases, indicating that ExoA incised a damaged duplex 5′ next to a damaged nucleotide. No specific cleavage was observed after incubation of ExoA with Tg·A, 8oxoG·C, εA·T, UG, 5 mC·G, or 5ohmC·G duplexes (Fig. 2, lanes 7, 11–13, and 15–16 and Fig. S2). Taken together, these results suggest that although *B. subtilis* AP endonuclease has a weak NIR activity (as compared to that of Nfo and APE1), it has broad DNA substrate specificity similar to that of

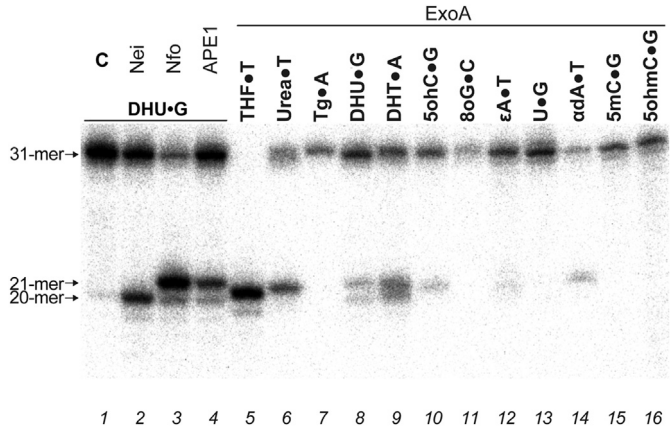

Fig. 2. DNA substrate specificity of *B. subtilis* ExoA. Denaturing PAGE analysis of ExoA incision activity on the 3′-end [^{32}P]-3′-dAMP-labeled oligonucleotide duplexes containing various DNA base lesions. Lanes 1–4, DHU·G incubated or not incubated with 50 nM Nei, 0.5 nM Nfo, and 0.5 nM APE1; Lanes 5–16, THF·T, Urea·T, Tg·T, DHU·G, DHT·A, 5ohC·G, 8oxoG·C, εA·T, U·G, αdA·T, 5 mC·G and 5 ohmC·G duplex oligonucleotides incubated in the presence of 1 nM ExoA for 10 min at 37 °C. Substrate and incision product sizes are indicated on the left. "C" indicates a control reaction without an enzyme. Products of the reaction were desalted prior to separation by denaturing PAGE. For details see Materials and Methods.

E. coli Nfo [41,42].

3.3. The presence of Mg^{2+} ion in APE1 crystal structures

The structural mechanism of NIR function of exonuclease III-related AP endonucleases is not well understood due to the absence of a published crystal structure of an enzyme complexed with NIR substrates. Therefore, we attempted to obtain the crystal structures of ExoA (see below) as well as the WT APE1 and APE1-D210 N mutant in complex with a 15-mer αdA-DNA or DHU-DNA. We obtained either DNA crystals or crystals of APE1 in complex with a truncated DNA duplex due to the exonuclease activity of APE1 [43], and/or a DNA-free enzyme. The DNA-free WT APE1 crystals were obtained in two crystal forms depending on the crystallization conditions. The form at pH 6.5 (form I), which was solved at high resolution (1.8 Å), is that of the first deposited structure with PDB code 1BIX [37] obtained at pH 6.2 with Sm^{2+} consisting of one molecule in the asymmetric unit. The second form obtained at pH 7.5 (form II), which was solved at 2.7 Å resolution, is that of the deposited structure with PDB code 4LND obtained at pH 6.5, and at 1.92 Å resolution consists of three molecules per asymmetric unit [44]. Although the crystallization conditions (70% MPD and 100 mM Hepes-KOH pH 7.5) of form II and the storage buffer (20 mM Hepes-KOH pH 7.5 and 50 mM KCl) of the purified APE1 were devoid of metal ions, the form II structure showed a single Mg^{2+} in the active site indicating that the enzyme has acquired an endogenous metal ion during the production of the enzyme in *E. coli*. We found that the Mg^{2+} ion interacts only with the side chains of D70 and E96. The lack of complete coordination may be due to the low metal occupancy because APE1 has trapped metal ions during its production in *E. coli*. Form I was solved under crystallization conditions including 200 mM of magnesium acetate. The resulting structure showed a single Mg^{2+} ion in the active site with remarkable coordination of ideal octahedral geometry formed by the two carboxylate groups D70 and E96 and four water molecules at distances of 1.9–2.1 Å, which are typical for Mg-oxygen bonds (Fig. S3). A similar octahedral metal coordination has been reported elsewhere in the same binding site referred as the "A" site in the three molecules of the asymmetric unit of the form II crystal (PDB code 4LND) and more recently in the single molecule of the asymmetric unit of a new crystal form obtained with the C138A-APE1 point mutant (PDB code 4QH9) [18,44]. A Mn^{2+} ion, instead of a Mg^{2+}, occupies the metal-binding site in 4QH9 [18]. Inspection of the electron density maps revealed no more metal-binding sites in the form I and form II structures, particularly around a putative second metal site named the "B site," where a second Pb^{2+} ion was found interacting with the side chains of D210, N212, and H309, which are the three essential catalytic residues [26]. Later on, it was shown that Pb^{2+} inhibits APE1 [45]. A water molecule occupies the position of the second Pb^{2+}, and this was observed in all DNA-free APE1 structures solved in the presence of a divalent metal ion bound in the A site. The well-coordinated Mg^{2+} showed a temperature factor of 32 Å^2, which is consistent with a fully occupied metal site, which interacts with the side chains of N68 and D308 through two water molecules involved in the octahedral coordination (Fig. S3).

3.4. Structure of the B. subtilis ExoA protein and structural comparison with E. coli ExoIII, Mth212 and APE1: identification of crucial amino acid residues in APE1

We next determined the crystal structure of the ExoA protein at 1.84 Å resolution by molecular replacement using the coordinates of human APE1 (PDB code 1BIX [37]) as a search model. Data collection and processing statistics are given in Table 1. We could not obtain the crystals of ExoA as a NIR complex. Structural comparison of ExoA with all other PDB entries using SSM-EBI (http://www.ebi.ac.uk/msd-srv/ssm) [46] indicated that ExoA has, as expected, the AP endonuclease fold derived from the *E. coli* ExoIII family. The structures most similar to our ExoA structure are the human APE1 (PDB code 1DEW) and archaeal Mth212 (PDB code 3G00) with a root mean square deviation (rmsd) ~1 Å over 245 and 250 Cα atoms, respectively. Its superposition with *E. coli* Xth yielded a rmsd of 1.6 Å (PDB code 1AKO) with 33% sequence identity. The active site of ExoA contains one well-defined Ca^{2+} ion coming from the crystallization conditions. The low *B*-factor of the metal (16.9 Å^2) implies full occupancy. The metal position and ligands were found to be essentially the same as those for the metal ion in APE1: N9 and E36 (equivalent to APE1 residues D70 and E96) and four water molecules (Fig. S3). Therefore, the metal ion bound in a single site is a common feature in exonuclease III family of AP endonucleases.

Both archaeal Mth212 and human APE1 have highly efficient NIR activities, whereas bacterial ExoA and Xth show weak and no NIR activities, respectively. In order to identify the residues responsible for the gain of NIR activity by APE1 and its absence in Xth, we superimposed and compared the three structures of human APE1 (PDB code 1DEW), archaeal Mth212 (PDB code 3G00), and ExoA with that of *E. coli* Xth (PDB code 1AKO) using COOT [39] and performed a structure-based sequence alignment with manual editing from a CLUSTAL alignment (Fig. 3A). As shown in Table 2, comparative analysis of the alignments revealed several amino acid residues involved in the active and DNA-binding sites that differ between NIR-proficient and NIR-deficient AP endonucleases. Among the nonconserved residues between Xth and the three other AP endonucleases, we focused on residues of the active site as well as those implicated in DNA binding, which are potentially important for the NIR activity. We identified four residues: N174 and G231 located in the active site pocket and another two involved in DNA binding: Y128 and T268 (APE1 numbering, Fig. 3B and S4). The equivalent residues of the two conserved residues N174 and G231 from the active site of NIR AP endonucleases are the bulkier residues Q112 and S178, respectively in Xth, making the active site pocket of Xth smaller than that of the three other AP enzymes; this

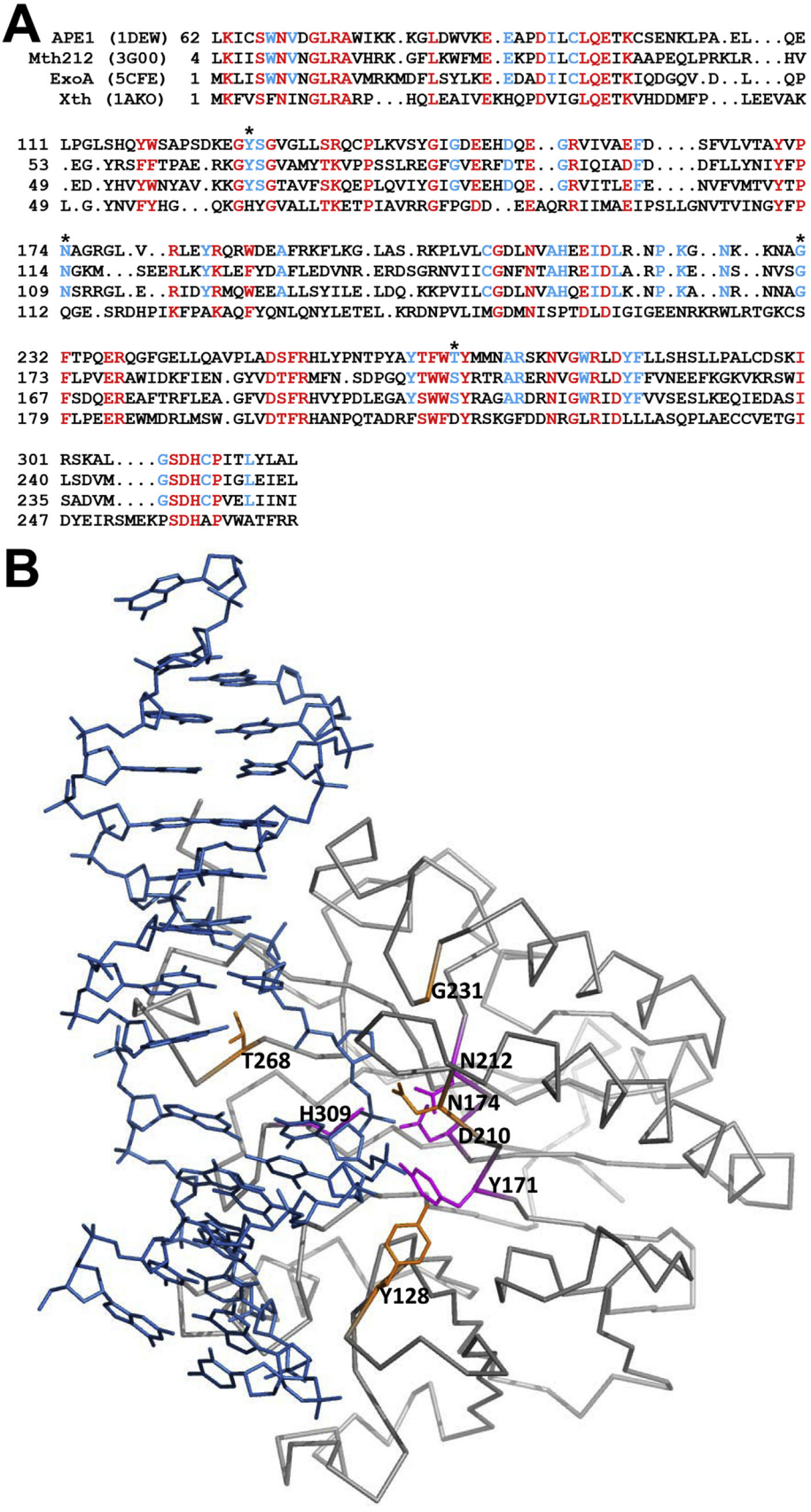

Fig. 3. Sequence alignments and structure of the APE1–DNA complex. (**A**) Structure-based sequence alignment of four Xth family AP endonucleases. Red color indicates the conserved amino acids for all proteins and blue color that for amino acids for APE1, Mth212, and ExoA proteins but not for Xth. *APE1 amino acids chosen for mutation analysis. (**B**) Ribbon representation of the APE1–DNA complex (PDB code 1DEW). The four residues labeled for mutagenesis and kinetic analysis are shown in sticks.

Table 2
Structural and functional roles of various amino acid residues in the exonuclease III family of AP endonucleases.

	Exonuclease III family AP endonucleases				Structural and functional roles
	APE1	ExoA	Mth212	Xth	
1	175–181	Similar to APE1	Practically absent	113–122	DNA insertion loop
2	G176	R111	K116	R113	DNA binding
3	R177 and M270	R112 and R204	M117 and R209	–R216	Insertion into DNA duplex and DNA locking
4	N222-N229	Similar to APE1	Similar to APE1	I163-K176	Small loop in APE1, ExoA, and Mth212 but big one in Xth (α_{15})
5	N222	N164	V170	K176	DNA contact
6	A230	A165	S171	C177	DNA binding
7	Y128	Y63	Y68	H62	DNA contact
8	T268	S202	S207	D214	Contact with 5′-phosphate of neighboring 3′ nucleotide of AP site
9	R185	R120	K125	K125	Possible contact with dUMP in active site
10	N174	N109	N114	Q112	Volume of active site pocket
11	G231	G166	G172	S178	Volume of active site pocket

situation should prevent a flipped out damaged base from being accommodated into the active site pocket. The side chain of N174 and the Cα of G231 are located at 2.47 and 4.20 Å distance from the O4′ and C1′ of the flipped out AP site, respectively. The conserved tyrosine, Y128, Y63, or Y68 in APE1, ExoA, and Mth212, respectively, is H62 in Xth. This tyrosine interacts with the phosphate group of the n-1 nucleotide of the AP site [47]. Replacing the tyrosine with a histidine can affect DNA binding due to the residue length and the position of protonated atom at physiological pH. Threonine at position 268 of APE1 is equivalent to serine in ExoA and Mth212, and to the acidic residue D214 in Xth. This T268 belongs to the loop region, which penetrates the DNA helix from the minor groove close to the AP site. Its side chain is sandwiched between the M270 side chain and the DNA phosphate backbone. It could interact with the 5′-phosphate group of the neighboring 3′-nucleotide of the AP site (n + 1). Modeling an aspartate at position 268 would affect the DNA binding either directly with the phosphate group of the DNA backbone due to repulsive charges or via the M270, which by moving avoids steric clashes with the side chain of T268 and could affect DNA distortion.

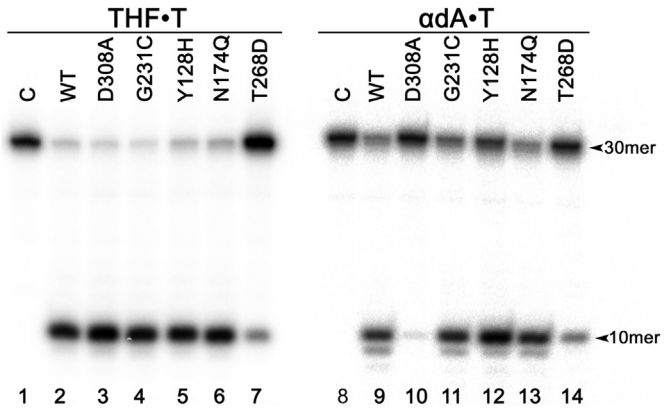

Fig. 4. Comparative characterization of AP site cleavage and NIR activities of APE1 mutants. 5′-[^{32}P]labeled 30-mer THF·T (100 nM) and αdA·T (10 nM) were incubated at 37 °C with 1 and 5 nM of the APE1 WT and mutant proteins for 5 min under BER conditions and for 10 min under NIR conditions, respectively. Products of the reaction were desalted prior to separation by denaturing PAGE. The arrow denotes the position of the 30-mer substrate and 10-mer cleavage product.

3.5. Biochemical characterization of the APE1 mutants

To examine the role of the nonconserved amino acid residues identified in the 3D alignment, we constructed and characterized four single point APE1 mutants Y128H, N174Q, G231S, and T268D. Because these substitutions make APE1 more similar to its *E. coli* ortholog, we expected that they would convert APE1 to a NIR-deficient AP endonuclease similar to Xth. All four APE1 mutant proteins were purified to homogeneity and analyzed for the following repair functions with the respective DNA substrates. AP endonuclease activity was measured by means of the THF·T duplex, and NIR endonuclease activity by means of duplexes αdA·T and DHU·G. It should be noted that for each distinct APE1-catalyzed DNA repair activity, we used specific reaction conditions. In addition, the previously characterized NIR- and 3′-exonuclease-deficient/BER-proficient APE-D308A mutant [34] together with wild-type APE1 served as negative and positive controls, respectively.

As shown in Fig. 4, all APE1 mutants could cleave the duplex oligonucleotide containing a synthetic AP site (THF); however, under BER assay conditions, the APE1-T268D mutant showed a lower AP endonuclease activity as compared to WT APE1 and other mutants including D308A (lane 7 *versus* lanes 2–6). As for the NIR activity, among APE1 mutants tested, only D308A and T268D showed a noticeable deficiency in the cleavage of the αdA·T duplex (lanes 10 and 14), as compared to that of WT (lane 9). These data suggest that amino acid residue T268 is necessary for both BER and NIR activities. In contrast, under non–steady-state reaction conditions other three APE1 mutants Y128H, N174Q, and G231S showed a more or less wild-type level of the BER and NIR activities (lanes 4–6 and 11–13).

Hydrolytic AP endonucleases, in addition to their AP site cleavage and NIR activities, also possess 3′-phosphatase and nonspecific 3′→5′ exonuclease functions to remove 3′-blocking phosphate residues and 3′-terminal regular nucleotides, respectively, in DNA strand breaks generated by ROS and repair enzymes [14,48]. To test whether the APE1 mutant proteins have the 3′→5′ exonuclease and 3′-phosphatase activities, we used the Exo20·T and Exo20^{P}·T duplex oligonucleotides containing one nucleotide and one nucleoside gap, respectively (Fig. S1). Results revealed that 0.2 nM WT APE1 removed more than 80% of 3′-terminal phosphate residues in the 3′-[^{32}P]labeled Exo20^{P}·T duplex in 10 min, indicating robust 3′-phosphatase activity (Fig. S5). All four APE1 mutants (Y128H, N174Q, G231S, and T268D) could remove 3′-phosphate residues but with somewhat lower efficiency as compared to WT APE1 at the same protein concentrations (Fig. S5).

APE1-Y128H and APE1-T268D mutants showed the lowest and highest 3′-phosphatase activity, respectively, as compared to the other two mutants. Regarding the 3′→5′ exonuclease activity, 4 nM WT APE1 could degrade more than 90% of 20-mer 5′-[^{32}P]labeled Exo20 in the Exo20·T duplex in 10 min at 37 °C under the experimental conditions used (Fig. S6). As expected, no significant exonuclease activity was observed when we used the control NIR-deficient APE1-D308A mutant. Unexpectedly, APE1-T268D showed only a 10-fold less efficient 3′→5′ exonuclease activity than WT APE1 did. On the other hand, the NIR-proficient APE1-Y128H

showed a decreased 3′→5′ exonuclease activity as compared to APE-WT, suggesting that NIR and exonuclease functions in APE1 could be mutationally separated. Except for APE1-Y128H, the NIR-proficient APE1 mutants (N174Q and G231S) were found to have approximately the same wild-type level of 3′→5′ exonuclease activity (Fig. S6).

3.6. Steady-state kinetic characterization of APE1 mutants

To quantify the observed differences in the repair activities of APE1 mutants, we measured steady-state kinetic parameters of the repair reactions and calculated the K_M, k_{cat}, and k_{cat}/K_M values for the WT APE1 and for the four relevant mutants. The following DNA substrates were used: the THF·T duplex to measure AP endonuclease activity under BER and NIR conditions; the αdA·T and the DHU·G duplexes to measure NIR activity under NIR conditions; and the Exo20^{THF}·T recessed duplex, containing THF at the 3′ end of a gap, to measure 3′-repair phosphodiesterase activity. As shown in Table 3, all four APE1 mutants tested, except G231S, showed reduced repair activities in comparison with the WT APE1 on one or several DNA substrates tested. For comparison, the kinetic parameters of APE1-D308A acting on the same DNA substrates were remeasured and the values (Table 3) were found to be similar to those obtained in our previous study [34]. The mutants can be subdivided into three groups by the degree of change in their DNA substrate specificity. The first group, which includes only the APE1-G231S mutant, showed virtually no changes in DNA repair activities as compared to WT APE1. The second group, containing mutants APE1-Y128H and N174Q, showed a significant but still minor reduction in the k_{cat}/K_M values for AP site cleavage under BER conditions (4- and 9-fold for Y128H and N174Q mutant, respectively, mainly due to the decrease in K_M values), NIR activity on DHU·G (6-fold for N174Q due to the decrease in k_{cat} value) and 3′-phosphodiesterase activity (3-fold for N174Q). In the third group, APE1-T268D and D308A mutants showed a dramatic 3700-fold reduction and no NIR activity on the αdA·T duplex, respectively, mainly due to the decrease in k_{cat}. In contrast to APE1-D308A, T268D yielded a strong (50-fold) reduction in the NIR activity on the DHU·G duplex due to the decrease in both K_M and k_{cat} *versus* only a 4-fold reduction observed with the D308A mutant.

It is noteworthy that the T268D-catalyzed AP site cleavage activity was found to have 10-fold higher efficiency under NIR conditions, whereas under BER conditions a 440-fold reduction was observed relative to WT APE1, mainly due to an increase and decrease in k_{cat} under NIR and BER conditions, respectively (Table 3). Similar to D308A, the T268D mutant also showed a moderate decrease (~7-fold) in the 3′-phosphodiesterase activity as compared to WT APE1. In summary, analysis of the kinetic parameters indicated that APE1-T268D is deficient in the NIR function on DNA substrates containing both α- and β-anomers of nucleotides, but can still perform BER: AP endonuclease and 3′-phosphodiesterase functions were observed at a low Mg^{2+} concentration.

3.7. Divalent metal ion dependence of AP endonuclease and NIR activities catalyzed by the APE1-T268D mutant

Previously, Masuda and colleagues and our laboratory showed that Mg^{2+} dependence of the APE1-catalyzed cleavage is sigmoidal with strong stimulation of the BER activity on an AP site and dramatic inhibition of the NIR activity on both DHU·G and αdA·T substrates at increasing concentrations of $MgCl_2$: from 0.1 to 10 mM [4,6,23]. A mutation of aspartate 283 to alanine results in the loss of sigmoidal Mg^{2+} dependence of AP site cleavage catalyzed by APE1-D283A [23]. Here, we examined the influence of $MgCl_2$ concentration on APE1-T268D-catalyzed BER and NIR functions. As shown in Fig. 5, cleavage activities of APE1-T268D toward an AP site and αdA·T also showed a strong Mg^{2+} dependence, but the metal activation profile was strikingly different from that of WT APE1. Indeed, the APE1-T268D mutant was found to have the highest AP endonuclease activity at low $MgCl_2$ (≤2 mM) and the lowest activity at high $MgCl_2$ concentration (≥10 mM) (Fig. 5). This activity profile is inverted in comparison with the Mg^{2+}-dependent profile of WT APE1 AP endonuclease activity [4,6,23]. In contrast, Mg^{2+}-dependent profile of the APE1-T268D-catalyzed cleavage of αdA·T was more similar to that of WT APE1 [4]. The mutant and wild-type APE1 showed the highest NIR activity at 0.5 and 1 mM $MgCl_2$, respectively, and both enzymes were strongly inhibited at a high $MgCl_2$ concentration (10 mM). The Mg^{2+}-dependent profile of APE1-T268D catalyzed AP site cleavage activity was in agreement with steady-state kinetic parameters of the mutant.

The unusual Mg^{2+}-dependent profile of APE1-T268D when acting upon an AP site may be due to the presence of an innate divalent metal ion in the protein [49]. Indeed, according to our

Table 3
Steady-state kinetic parameters of the WT and mutant APE1 proteins.

DNA substrate[a]	APE1 WT		APE1 G231S		APE1 Y128H		APE1 N174Q		APE1 T268D		APE1 D308A	
	K_M, nM	k_{cat}, min^{-1}	K_M, nM	k_{cat}, min^{-1}	K_M, nM	k_{cat}, min^{-1}	K_M, nM	k_{cat}, min^{-1}	K_M, nM	k_{cat}, min^{-1}	K_M, nM	k_{cat}, min^{-1}
THF·T[b]	0.5	0.17	0.72	0.35	1.2	0.22	0.78	0.28	0.79	2.7	0.92	0.55
THF·T[c]	7.7	97	18	200	37	110	27	37	78	2.2	11	70
αdA·T[b]	1.6	1.5	1.0	1.0	2.3	0.9	1.5	0.7	12	0.003	None	None
DHU·G	29	0.31	9.4	0.066	25	0.31	25	0.045	110	0.024	8.6	0.025
Exo20^{THF}·T	6.0	20	6.4	23	7.4	16	9.3	10	85	42	4.3	1.3

DNA[a]	APE1 WT	Fold decrease of k_{cat}/K_M value in APE1 mutants compared to WT				
	k_{cat}/K_M, min^{-1}·M^{-6}	APE1 G231S	APE1 Y128H	APE1 N174Q	APE1 T268D	APE1 D308A
THF·T[b]	340	0.70	1.9	0.95	0.10	0.57
THF·T[c]	12,700	1.1	4.3	9.14	440	2.0
αdA·T[b]	940	0.94	2.4	2.0	3700	∞
DHU·G	11	1.5	0.86	5.9	50	3.7
Exo20^{THF}·T	3300	0.95	1.6	3.0	6.8	11

[a] Each type of DNA substrate was used to measure a specific APE1 activity under appropriate optimal reaction conditions: THF·T for AP endonuclease activity; αdA·T and DHU·G for NIR activity; Exo20^{THF}·T for 3′-repair diesterase activity (see Materials and Methods). To determine K_M and k_{cat}, the linear velocity was measured, and the constants were calculated using Lineweaver-Burk plots. Standard deviations for K_M and k_{cat} values varied within 20–40%. None = no activity was detected under these experimental conditions.

[b] NIR reaction conditions were used for the AP endonuclease assay.

[c] Standard AP endonuclease reaction conditions were used for the AP endonuclease assay.

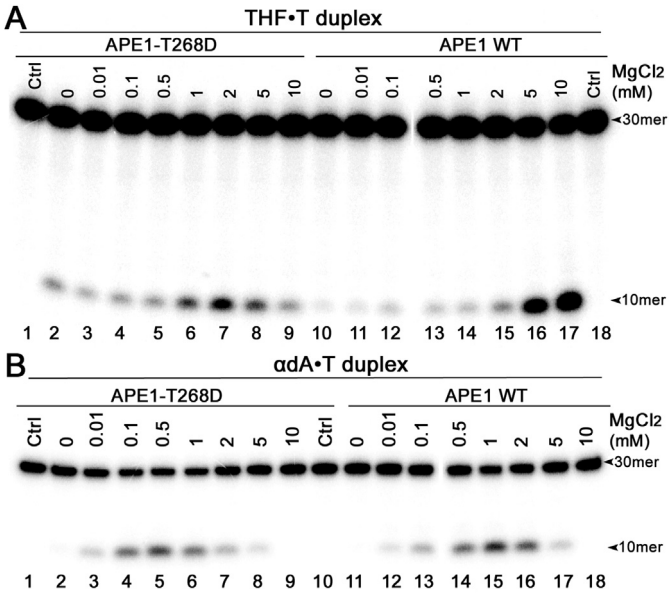

Fig. 5. Magnesium-dependent activity profiles of the APE1-T268D mutant and APE1-WT. (**A**) AP endonuclease activity of 0.5 nM APE1-T268D and APE1-WT toward 100 nM 5′-[^{32}P]labeled 30-mer THF·T duplex, in the presence of varying $MgCl_2$ concentrations in the buffer consisting of 20 mM Hepes-KOH pH 7.6, 50 mM KCl, and 0.1 mg mL^{-1} BSA for 5 min at 37 °C. Lanes 1 and 18, control untreated duplexes; lanes 2–9, THF·T incubated with 0.5 nM APE1-T268D in the presence of 0, 0.01, 0.1, 0.5, 1, 2, 5, or 10 mM $MgCl_2$; lanes 10–17, THF·T incubated with 0.5 nM APE1-WT in the presence of 0, 0.01, 0.1, 0.5, 1, 2, 5, or 10 mM $MgCl_2$. (**B**) NIR activity of 10 nM APE1-T268D and 2 nM APE1-WT toward 10 nM 5′-[^{32}P]labeled 30-mer αdA·T duplex, in the presence of varying $MgCl_2$ concentrations in the buffer consisting of 20 mM Hepes-KOH pH 7.6, 50 mM KCl, and 0.1 mg mL^{-1} BSA for 10 min at 37 °C. Lanes 1 and 10, control untreated duplexes; lanes 2–9, αdA·T incubated with 0.5 nM APE1-T268D in the presence of 0, 0.01, 0.1, 0.5, 1, 2, 5, or 10 mM $MgCl_2$; lanes 11–18, αdA·T incubated with 2 nM APE1-WT in the presence of 0, 0.01, 0.1, 0.5, 1, 2, 5, or 10 mM $MgCl_2$. Products of the reaction were desalted prior to separation by denaturing PAGE. The arrow denotes the position of the 30-mer substrate and 10-mer cleavage product.

crystallographic data, APE1 could chelate divalent metal ion contaminants from the buffer solutions without added Mg^{2+}, which were used for the purification steps and reactions with DNA. To examine this phenomenon, we incubated the APE1 WT and T268D mutant proteins with 10 mM EDTA in order to pull out all metal cations present in the proteins. After that, the enzymes were diluted more than 1000-fold with the buffer without divalent metal ions and these dilutions were tested for the AP endonuclease and NIR activities in the reaction buffers containing varied amounts of $MgCl_2$ (0–10 mM). As shown in Fig. 6A and B, the APE1-T268D mutant treated or not treated with EDTA showed the highest activity on the THF·T duplex in the presence of 1 mM $MgCl_2$ (Fig. 6A, lanes 4 and 8), but was strongly inhibited by 10 mM $MgCl_2$ (lanes 5 and 9). In contrast, the APE1-WT protein treated or not treated with 10 mM EDTA was found to have the highest activity on the THF·T duplex in the presence of 10 mM $MgCl_2$ (Fig. 6A, lanes 14 and 18 and Fig. 6B) but was strongly inhibited at a low concentration of $MgCl_2$ (1 mM; Fig. 6A, lanes 13 and 17 and Fig. 6B). Thus overall, incubation of the APE1 WT and T268D mutant proteins in the buffer containing a high concentration of a metal-chelating agent did not lead to the statistically significant changes in the profile of Mg^{2+} dependence of the AP site cleavage activity catalyzed by APE1, as compared to the control APE1 proteins incubated in buffer without EDTA and metal cations (Fig. 6B).

We also determined whether incubation of the APE1-T268D mutant with EDTA has an effect on the NIR activity. As shown in Fig. 6C, both the EDTA-treated and untreated APE1-T268D mutants catalyzed cleavage of the αdA·T duplex in the presence of 0.1 mM $MgCl_2$ with similar efficiency values (lanes 2–4 *versus* 6–8). EDTA-treated and untreated APE1-T268D mutants were found to cleave αdA·T even in the absence of any added metal cations, although with negligible efficiency (lanes 5 and 9), suggesting that APE1 in which all metal cations are removed by EDTA treatment can still use some divalent metal ions contaminants that may be present at extremely low concentrations in the reaction buffers without added $MgCl_2$. In conclusion, all these results suggest that removal of all metal cations from the proteins did not significantly influence the Mg^{2+} dependence of the APE1-WT and APE1-T268D mutant. Therefore, we believe that the inverted Mg^{2+} dependence of AP site cleavage activity catalyzed by APE1-T268D is not due to the presence of an innate metal cation in the protein.

4. Discussion

4.1. NIR activity of BsExoA and critical residues in Xth family NIR-AP endonucleases

In the present work, we studied the NIR activities of *B. subtilis* and human AP endonucleases using structural analysis coupled to biochemical and mutational studies. The ability of spores of *B. subtilis* to survive during long periods of metabolic dormancy points to the existence of highly efficient DNA repair pathways that can deal with genomic lesions caused by long-term exposure to environmental factors [50]. Here, we further characterized the DNA substrate specificity of the *B. subtilis* Xth family AP endonuclease ExoA and solved its crystal structure. Our results show that ExoA, in addition to BER functions, has a weak NIR activity toward α-anomeric nucleotides and several oxidized pyrimidines in duplex oligonucleotides. We found that the *E. coli* ortholog of ExoA, the Xth protein, does not have a NIR function; instead, in *E. coli*, a second AP endonuclease (Nfo) can catalyze the cleavage of the αdA·T duplex [8,10]. Genetic studies showed that spores lacking both BsNfo and ExoA show dramatically slowed germination and outgrowth and increased spontaneous and H_2O_2-induced mutation frequency, suggesting that both AP endonucleases are necessary for repair of abasic sites and oxidized DNA bases *in vivo* [28]. Furthermore, BsNfo and ExoA might play a role in counteracting DNA base damage induced by UV light and ionizing radiation [31]. On the basis of these observations, we believe that the ability of ExoA to repair oxidatively damaged DNA bases serves as a backup activity to BsNfo which most likely also have an NIR function.

Superimposition of the crystal structures of ExoA, Xth, Mth212, and APE1 revealed differences between the NIR-deficient Xth and the NIR-proficient AP endonucleases APE1, Mth212, and ExoA. For example, the active sites of NIR AP endonucleases contain the conserved residues asparagine-174 and glycine-231, whereas in Xth, these residues are replaced by bulkier glutamine-112 and serine-178 residues, thus making the active site of *E. coli* AP endonuclease smaller than that of APE1, Mth212, and ExoA. Threonine-268 in APE1 (S202 and S207 in ExoA and Mth212, respectively), which participates in contacts with the 5′-phosphate residue of the neighboring 3′-nucleotide to AP site, is replaced by the negatively charged D214 residue in Xth. This finding is suggestive of potential differences in specific DNA-protein interactions between NIR-proficient and NIR-deficient AP endonucleases.

Here, by introducing single amino acid changes N174Q, G231S, Y128H, or T268D into APE1, which correspond to the evolutionary changes that occurred between *E. coli* and human enzymes, we expected that these APE1 Xth-like mutants would be NIR-deficient. Nonetheless, the detailed biochemical characterization of the DNA substrate specificity of the mutants showed that only one out of the four APE1 mutants, namely T268D, substantially lost NIR activities (Fig. 4 and Table 3). The T268D substitution might strongly perturb

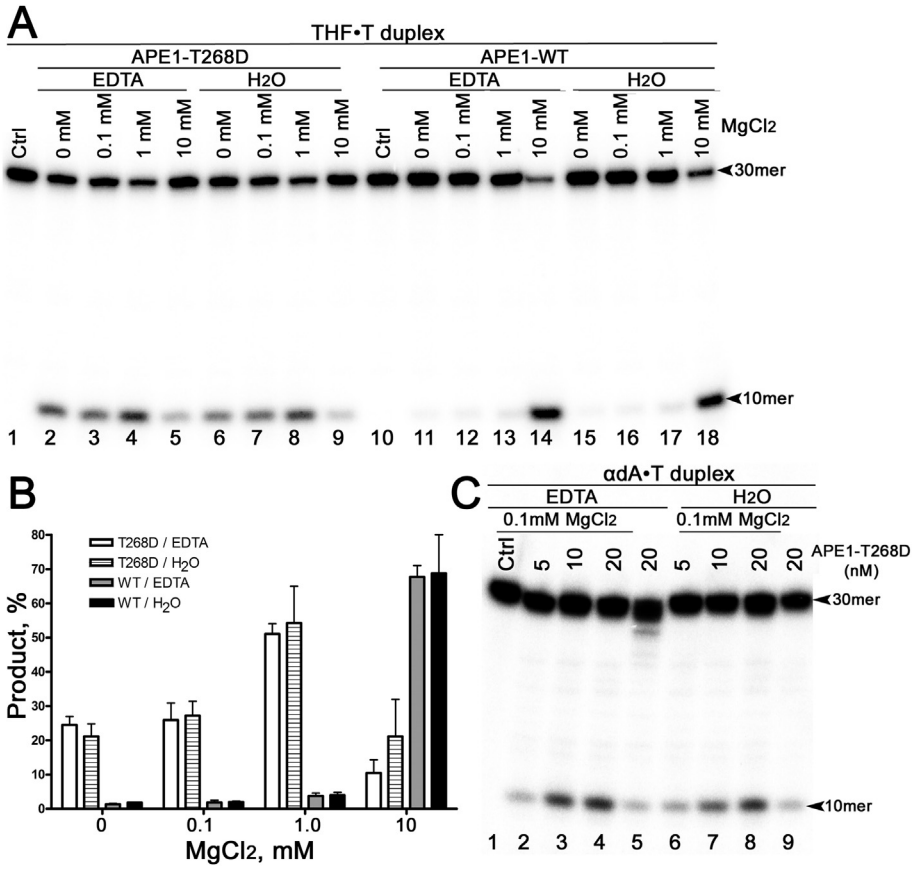

Fig. 6. Effects of incubation of APE1-WT or APE1-T268D mutant with 10 mM EDTA on their AP endonuclease and NIR activities. (**A**) Magnesium-dependent AP site cleavage activity profiles of EDTA-treated and untreated APE1-WT and APE1-T268D mutant. The 5′-[^{32}P]labeled 30-mer THF·T duplex (10 nM) was incubated with 0.5 nM APE1-T268D or APE1-WT, in the presence of varying $MgCl_2$ concentrations in the buffer consisting of 20 mM Hepes-KOH pH 7.6, 50 mM KCl and 0.1 mg mL^{-1} BSA for 5 min at 37 °C. Lanes 1 and 10, control untreated duplexes; lanes 2–5, EDTA-treated APE1-T268D in the presence of 0, 0.1, 1, or 10 mM $MgCl_2$; lanes 2–5, untreated APE1-T268D in the presence of 0, 0.1, 1, or 10 mM $MgCl_2$; lanes 11–14, EDTA-treated APE1-WT in the presence of 0, 0.1, 1, or 10 mM $MgCl_2$; lanes 15–18, untreated APE1-WT in the presence of 0, 0.1, 1, or 10 mM $MgCl_2$. (**B**) Graphical representation of the data in panel A. (**C**) NIR activity of EDTA-treated and untreated APE1-T268D mutant. The 5′-[^{32}P]labeled 30-mer αdA·T duplex (10 nM) was incubated with 5–20 nM APE1-T268D, in the absence or presence of 0.1 mM $MgCl_2$ in the buffer consisting of 20 mM Hepes-KOH pH 7.6, 50 mM KCl, and 0.1 mg mL^{-1} BSA for 10 min at 37 °C. Lane 1, control untreated duplex; lanes 2–5, 5, 10, or 20 nM EDTA-treated APE1-T268D in the presence of 0.1 and 0 mM $MgCl_2$; lanes 6–9, 5, 10, or 20 nM untreated APE1-T268D in the presence of 0.1 and 0 mM $MgCl_2$. Products of reaction were desalted prior to separation by denaturing PAGE. The arrow denotes the position of the 30-mer substrate and the 10-mer cleavage product.

the APE1 interactions with DNA via electrostatic repulsion and its interference with M270 loop insertion in the DNA minor groove. It was shown that the substitution of amino acid residues M270 and M271 with alanine does not decrease the AP site cleavage activity of APE1, indicating that these residues do not participate in the abasic nucleotide flipping [22]. Because T268 belongs to the same loop region of M270 and M271, it probably does not participate in the flipping mechanism. The presence of high concentrations of metal ions leads to a very low catalytic efficiency of the T268D mutant in terms of AP site cleavage, meaning that combining an aspartate at position 268 with metal ions affects the binding of DNA substrate or/and the stability of the enzyme–substrate complex.

In agreement with our previous observations, both the NIR endonuclease activity on αdA·T and the exonuclease activity on nicked duplex DNA are concurrently reduced in the APE1-T268D mutant (Fig. 4 and S6), thus further supporting the observations that NIR and exonuclease functions are likely to be mechanistically linked in NIR AP endonucleases [4,51]. Nonetheless, APE1-T268D shows only a ~10-fold reduction in the 3′→5′ exonuclease activity as compared to WT APE1. Furthermore, the NIR-proficient APE1-Y128H mutant has a moderately decreased 3′→5′ exonuclease activity, suggesting that NIR and exonuclease functions in APE1 can be at least partially mutationally separated. The substitutions N174Q and G231S, which considerably reduce the volume of the active site pocket of APE1, prevent the accommodation and recognition of a flipped out DNA base. The analysis of kinetic constants did not reveal dramatic changes in the DNA substrate specificity of APE1-N174Q, and especially of the G231S mutant, as compared to WT APE1. These data confirm that the active site pocket cannot bind a flipped out damaged base as suggested by the APE1–DNA structures with an AP site. Therefore, using mutagenesis and kinetic studies, we provide new lines of evidence that NIR activity takes place without a classical base flipping mechanism. At present, the molecular basis of recognition of the damaged base by AP endonucleases remains unclear due to the absence of a structure of a damage recognition complex. However, it is tempting to hypothesize that NIR-AP endonucleases recognize DNA damage via changes in the sugar puckering and in the distance between two neighboring phosphates in the DNA backbone at the site of the lesion. These phenomena in turn may also depend on the overall flexibility and dynamics of the DNA substrate and the enzyme.

4.2. The metal-binding site

Divalent metal ions play an essential role in AP endonuclease-catalyzed DNA repair activities such as protein stability, APE1-

substrate interaction, and catalysis [18,23,49]. It should be noted that in the absence of added Mg^{2+} and chelating agents in the *in vitro* kinetic assays, APE1 can still retain metal ions in its metal binding site during the protein production in *E. coli;* this state of affairs enables the enzyme to be catalytically active under these conditions. Various studies showed that this robust activity can be fully suppressed by rigorous chelation of Mg^{2+}, indicating that this cofactor is necessary for catalysis [52,53]. Several structural and mutational studies have pointed to the existence of alternative conformations of APE1: with a second metal-binding site referred to as site "B" [26,54]. Furthermore, based on molecular dynamics simulation of APE1 bound to an AP site of DNA, it has been proposed that Mg^{2+} may move between the two metal-binding sites during the reaction: from precleavage site "B" to product retention site "A" [55]. Two recent structural studies on the role of the metal in APE1 revealed that a single metal-binding site is present in APE1: the Mg^{2+} ion cannot bind to the B site, and movement of Mg^{2+} between sites A and B is inappropriate as catalytic evidence because the B site is located in the active site very closely to the three crucial catalytic residues [18,44]. Here, the two solved crystal forms (I and II) from the same batch of purified APE1 (obtained under different crystallization conditions: acidic and basic pH conditions/with and without metal, respectively) revealed a single bound Mg^{2+} in the expected site. The finding of a very well-coordinated metal in form I just as in PDB codes 4LND (form II with Mg^{2+}), 4QH9 (form III with Mn^{2+}), and 4QHE (form III with Mg^{2+}), correlates with diffraction at very high resolution (below 2 Å) and a role of a metal in protein stabilization. The presence of the single metal ion in the active site of APE1 regardless of pH is also validated by our two crystal structures. The 4QH9 structure shows two partially occupied Mg^{2+} sites that are 0.7 Å apart: one involving coordination primarily with E96 (A site, 0.35 occupancy) and the second involving coordination with both D70 and E96 (B site, 0.65 occupancy). The designations of A and B in this context refer to alternate positions of the Mg^{2+} cation. The presence of two partial sites for metal indicates that the metal can be mobile just as the E96 side chain for which three conformations have been observed [18]. In our form I structure, the conformation of E96 corresponds to that for the A site in 4QHE, which is different from that of the B site, which resembles that in 4QH9 (Mn^{2+}) and 4LND (form II Mg^{2+}). The single preformed metal-binding site in APE1 involving D70, E96, and, to a lesser extent, D308 in the endonuclease activity is necessary for stabilization of the enzyme alone and of the DNA product complex with the O3′ leaving group. Indeed, a structural comparison between Nfo and APE1 bound to a DNA forming a product complex with a single Mg^{2+} ion combined with mutagenesis kinetic analysis revealed that D210 and D212 coordinate the catalytic water molecule responsible for DNA cleavage. Moreover, ExoA contains an identical preformed metal-binding site in which the conserved glutamate confers plasticity to the active site, thus giving a metal ion flexibility in the active site.

4.3. N-terminal amino acid residues of APE1 and APE1-T268D mutant

The first 42 N-terminal disordered amino acid residues of APE1 are highly enriched in positively charged basic lysine and arginine residues, which can engage in electrostatic interactions with DNA phosphates. Recently, Tell and coworkers demonstrated that the first 33 amino acid residues mediate the binding of APE1 to RNA and to negative calcium responsive sequence elements (nCaRE) of certain gene promoters [56,57]. The deletion, mutation, and/or acetylation of lysine residues among the first 33 amino acid residues of APE1 lead to increased AP site cleavage activity [56,58], whereas deletion of the first N-terminal 61 amino acid residues results in a dramatic decrease of the NIR activity [6]. This result suggests that, these potential additional interactions of the N-terminal amino acid residues of APE1 with DNA in the presence of low concentrations of Mg^{2+} promote NIR activity, whereas at high Mg^{2+} concentrations (BER conditions), these disrupted interactions lead to an increased rate of enzymatic cleavage of the AP site. The dramatic 440-fold decrease in the kinetic efficiency (k_{cat}/K_M) in terms of AP site cleavage in APE1-T268D suggests that under BER conditions, the DNA-binding mode of the mutant is strongly affected. According to all these observations, we can hypothesize that the APE1-T268D mutant reveals the contribution of the N-terminal domain to the protein-DNA substrate interaction, which in turn under NIR conditions enables the mutant enzyme to cleave an AP site in duplex DNA with a 10-fold higher kinetic efficiency as compared to the WT enzyme. In line with this notion, Mg^{2+} dependence of BER and NIR activities of the APE1-T268D mutant showed analogous profiles, which are similar to that of the WT APE1 for NIR activity, supporting a cooperative effects of the N- and C-terminal DNA-binding sites on DNA incision activities, being both necessary for the NIR DNA substrates.

4.4. The NIR function signature

To find out whether the role of the APE1 T268 residue is conserved beyond the enzymes characterized in this study, we performed a multiple sequence alignment using amino acid sequences from recently characterized exonuclease III-related proteins (Fig. S7), such as prokaryotic enzymes (*Mycobacterium tuberculosis* MtbXthA and *Neisseria meningitides* NApe and NExo) and plant enzyme (*Arabidopsis thaliana* atARP). MtbXthA lacks a NIR activity [27], whereas AtARP has a robust NIR activity toward the αdA·T duplex (*our unpublished observation*). The protein sequence alignment shows that NIR-deficient EcXth and MtbXthA contain an aspartic acid residue at the position corresponding to T268 in APE1, whereas NIR-proficient plant ARP contains a glycine there. According to the known crystal structure of NApe [59] and the sequence homology with APE1, we believe that NApe and NExo may be NIR-proficient and deficient AP endonucleases, respectively. Therefore, one could use the presence of an aspartic residue *versus* a noncharged serine, threonine, or glycine residue in Xth-like AP endonucleases as a possible hallmark for NIR deficiency and NIR proficiency among exonuclease III-like AP endonucleases, respectively.

In conclusion, taken together, these results show that (*i*) exonuclease III family AP endonucleases from gram-positive bacteria have NIR functions with conserved amino acid residues involved in the removal of oxidatively damaged DNA bases, underlying the evolutionary conserved role of NIR function; (*ii*) structural analysis coupled to biochemical characterization of APE1 mutants reveal that amino acid residues in the active site pocket are not involved in the interactions with damaged DNA bases; (*iii*) structure-function analysis allows for mutational separation of conserved repair activities in AP endonucleases. These phenomena in turn form the basis for studies on the biological role of NIR function in the fight against potentially lethal DNA lesions generated by oxidative stress.

Conflict of interest

The authors declare that they have no conflict of interest.

Author contributions

M.R-R., I.G., A.M., D.A., Z.K., Z.A., A.M., and A.A.I. conducted all of the biochemical and mutational experiments. A.V. and S.M.

performed all the crystallography work. M.R.-R., B.T.M., A.A.I., and S.M. performed all alignments and structural analysis. M.R.-R., M.S., A.A.I., and S.M. designed all the experiments. M.R.-R., M.S., A.A.I., and S.M. wrote the manuscript. All the authors discussed the results and contributed to the writing of the manuscript.

Accession codes

Coordinates and structure factors of ExoA and APE1 have been deposited in the Protein Data Bank database under accession codes 5CFE and 5CFG for ExoA and APE1, respectively.

Acknowledgments

We acknowledge SOLEIL for provision of synchrotron radiation facilities for use of beamlines Proxima I (proposal ID 20110613) and Proxima II (proposal ID 20130869). In addition, we wish to thank Dr. Olga Lavrik for the recombinant Tdp1 protein. This work has benefited from the I2BC crystallization platform, supported by FRISBI ANR-10-INSB-05-01 and grants from la Ligue Nationale Française Contre le Cancer « Equipe LNCC 2016 » and Electricité de France RB 2016-17 to M.S., Fondation de France 2012-00029161 and Centre National de la Recherche Scientifique PRC CNRS-RFBR REDOBER 16-54-150004) to A.A.I., Science Committee of the Ministry of Education and Science of the Republic of Kazakhstan, Program 0212/PTF-14-OT and grant 3755/GF4 to B.T.M. M.R.-R. and I.G. were supported by postdoctoral fellowships from the Association pour la Recherche sur le Cancer [P2009] and [PDF20101202141], respectively.

Appendix A. Supplementary data

Supplementary data related to this article can be found at http://dx.doi.org/10.1016/j.biochi.2016.06.011.

References

[1] T. Lindahl, Instability and decay of the primary structure of DNA, Nature 362 (1993) 709–715.
[2] J. Cadet, T. Douki, D. Gasparutto, J.L. Ravanat, Oxidative damage to DNA: formation, measurement and biochemical features, Mutat. Res. 531 (2003) 5–23.
[3] J.H. Hoeijmakers, DNA damage, aging, and cancer, N. Engl. J. Med. 361 (2009) 1475–1485.
[4] S. Daviet, S. Couve-Privat, L. Gros, K. Shinozuka, H. Ide, M. Saparbaev, A.A. Ishchenko, Major oxidative products of cytosine are substrates for the nucleotide incision repair pathway, DNA Repair (Amst) 6 (2007) 8–18.
[5] M. Redrejo-Rodriguez, C. Saint-Pierre, S. Couve, A. Mazouzi, A.A. Ishchenko, D. Gasparutto, M. Saparbaev, New insights in the removal of the hydantoins, oxidation product of pyrimidines, via the base excision and nucleotide incision repair pathways, PLoS One 6 (2011) e21039.
[6] L. Gros, A.A. Ishchenko, H. Ide, R.H. Elder, M.K. Saparbaev, The major human AP endonuclease (Ape1) is involved in the nucleotide incision repair pathway, Nucleic Acids Res. 32 (2004) 73–81.
[7] H.E. Krokan, M. Bjoras, Base excision repair, cold spring harb, Perspect. Biol. 5 (2013) a012583.
[8] A.A. Ischenko, M.K. Saparbaev, Alternative nucleotide incision repair pathway for oxidative DNA damage, Nature 415 (2002) 183–187.
[9] D.O. Zharkov, Base excision DNA repair, Cell. Mol. Life Sci. 65 (2008) 1544–1565.
[10] H. Ide, K. Tedzuka, H. Shimzu, Y. Kimura, A.A. Purmal, S.S. Wallace, Y.W. Kow, Alpha-deoxyadenosine, a major anoxic radiolysis product of adenine in DNA, is a substrate for Escherichia coli endonuclease IV, Biochemistry 33 (1994) 7842–7847.
[11] A.A. Ishchenko, H. Ide, D. Ramotar, G. Nevinsky, M. Saparbaev, Alpha-anomeric deoxynucleotides, anoxic products of ionizing radiation, are substrates for the endonuclease IV-type AP endonucleases, Biochemistry 43 (2004) 15210–15216.
[12] A.A. Ishchenko, E. Deprez, A. Maksimenko, J.C. Brochon, P. Tauc, M.K. Saparbaev, Uncoupling of the base excision and nucleotide incision repair pathways reveals their respective biological roles, Proc. Natl. Acad. Sci. U. S. A. 103 (2006) 2564–2569.
[13] J. Georg, L. Schomacher, J.P. Chong, A.I. Majernik, M. Raabe, H. Urlaub, S. Muller, E. Ciirdaeva, W. Kramer, H.J. Fritz, The Methanothermobacter thermautotrophicus ExoIII homologue Mth212 is a DNA uridine endonuclease, Nucleic Acids Res. 34 (2006) 5325–5336.
[14] B. Demple, L. Harrison, Repair of oxidative damage to DNA: enzymology and biology, Annu. Rev. Biochem. 63 (1994) 915–948.
[15] S. Couve-Privat, A.A. Ishchenko, J. Laval, M. Saparbaev, Nucleotide incision repair: an alternative and ubiquitous pathway to handle oxidative DNA damage, in: Mark D. Evans, Marcus S. Cooke (Eds.), Oxidative Damage to Nucleic Acids, ©2007 Landes Bioscience and Springer Science+Business Media, Austin, 2007.
[16] T. Barnes, W.C. Kim, A.K. Mantha, S.E. Kim, T. Izumi, S. Mitra, C.H. Lee, Identification of Apurinic/apyrimidinic endonuclease 1 (APE1) as the endoribonuclease that cleaves c-myc mRNA, Nucleic Acids Res. 37 (2009) 3946–3958.
[17] C.D. Mol, D.J. Hosfield, J.A. Tainer, Abasic site recognition by two apurinic/apyrimidinic endonuclease families in DNA base excision repair: the 3' ends justify the means, Mutat. Res. 460 (2000) 211–229.
[18] H. He, Q. Chen, M.M. Georgiadis, High-resolution crystal structures reveal plasticity in the metal binding site of apurinic/apyrimidinic endonuclease I, Biochemistry 53 (2014) 6520–6529.
[19] D.M. Wilson 3rd, D. Barsky, The major human abasic endonuclease: formation, consequences and repair of abasic lesions in DNA, Mutat. Res. 485 (2001) 283–307.
[20] D.J. Hosfield, Y. Guan, B.J. Haas, R.P. Cunningham, J.A. Tainer, Structure of the DNA repair enzyme endonuclease IV and its DNA complex: double-nucleotide flipping at abasic sites and three-metal-ion catalysis, Cell 98 (1999) 397–408.
[21] E.D. Garcin, D.J. Hosfield, S.A. Desai, B.J. Haas, M. Bjoras, R.P. Cunningham, J.A. Tainer, DNA apurinic-apyrimidinic site binding and excision by endonuclease IV, Nat. Struct. Mol. Biol. 15 (2008) 515–522.
[22] C.D. Mol, T. Izumi, S. Mitra, J.A. Tainer, DNA-bound structures and mutants reveal abasic DNA binding by APE1 and DNA repair coordination [corrected], Nature 403 (2000) 451–456.
[23] Y. Masuda, R.A. Bennett, B. Demple, Rapid dissociation of human apurinic endonuclease (Ape1) from incised DNA induced by magnesium, J. Biol. Chem. 273 (1998) 30360–30365.
[24] K.M. Chou, Y.C. Cheng, The exonuclease activity of human apurinic/apyrimidinic endonuclease (APE1). Biochemical properties and inhibition by the natural dinucleotide Gp4G, J. Biol. Chem. 278 (2003) 18289–18296.
[25] C.M. Kane, S. Linn, Purification and characterization of an apurinic/apyrimidinic endonuclease from HeLa cells, J. Biol. Chem. 256 (1981) 3405–3414.
[26] P.T. Beernink, B.W. Segelke, M.Z. Hadi, J.P. Erzberger, D.M. Wilson 3rd, B. Rupp, Two divalent metal ions in the active site of a new crystal form of human apurinic/apyrimidinic endonuclease, Ape1: implications for the catalytic mechanism, J. Mol. Biol. 307 (2001) 1023–1034.
[27] S. Abeldenov, I. Talhaoui, D.O. Zharkov, A.A. Ishchenko, E. Ramanculov, M. Saparbaev, B. Khassenov, Characterization of DNA substrate specificities of apurinic/apyrimidinic endonucleases from Mycobacterium tuberculosis, DNA Repair (Amst) 33 (2015) 1–16.
[28] J.R. Ibarra, A.D. Orozco, J.A. Rojas, K. Lopez, P. Setlow, R.E. Yasbin, M. Pedraza-Reyes, Role of the Nfo and ExoA apurinic/apyrimidinic endonucleases in repair of DNA damage during outgrowth of Bacillus subtilis spores, J. Bacteriol. 190 (2008) 2031–2038.
[29] T. Shida, T. Ogawa, N. Ogasawara, J. Sekiguchi, Characterization of Bacillus subtilis ExoA protein: a multifunctional DNA-repair enzyme similar to the Escherichia coli exonuclease III, Biosci. Biotechnol. Biochem. 63 (1999) 1528–1534.
[30] J.M. Salas-Pacheco, B. Setlow, P. Setlow, M. Pedraza-Reyes, Role of the Nfo (YqfS) and ExoA apurinic/apyrimidinic endonucleases in protecting Bacillus subtilis spores from DNA damage, J. Bacteriol. 187 (2005) 7374–7381.
[31] R. Moeller, P. Setlow, M. Pedraza-Reyes, R. Okayasu, G. Reitz, W.L. Nicholson, Role of the Nfo and ExoA apurinic/apyrimidinic endonucleases in radiation resistance and radiation-induced mutagenesis of Bacillus subtilis spores, J. Bacteriol. 193 (2011) 2875–2879.
[32] A.A. Ishchenko, G. Sanz, C.V. Privezentzev, A.V. Maksimenko, M. Saparbaev, Characterisation of new substrate specificities of *Escherichia coli* and *Saccharomyces cerevisiae* AP endonucleases, Nucleic Acids Res. 31 (2003) 6344–6353.
[33] N.A. Lebedeva, N.I. Rechkunova, A.A. Ishchenko, M. Saparbaev, O.I. Lavrik, The mechanism of human tyrosyl-DNA phosphodiesterase 1 in the cleavage of AP site and its synthetic analogs, DNA Repair (Amst) 12 (2013) 1037–1042.
[34] A. Gelin, M. Redrejo-Rodriguez, J. Laval, O.S. Fedorova, M. Saparbaev, A.A. Ishchenko, Genetic and biochemical characterization of human AP endonuclease 1 mutants deficient in nucleotide incision repair activity, PLoS One 5 (2010) e12241.
[35] W.J. Kabsch, Automatic processing of rotation diffraction data from crystals of initially unknown symmetry and cell constants, J. Appl. Cryst. 26 (1993) 795–800.
[36] A.J. McCoy, R.W. Grosse-Kunstleve, P.D. Adams, M.D. Winn, L.C. Storoni, R.J. Read, Phaser crystallographic software, J. Appl. Crystallogr. 40 (2007) 658–674.
[37] M.A. Gorman, S. Morera, D.G. Rothwell, E. de La Fortelle, C.D. Mol, J.A. Tainer, I.D. Hickson, P.S. Freemont, The crystal structure of the human DNA repair endonuclease HAP1 suggests the recognition of extra-helical deoxyribose at DNA abasic sites, Embo J. 16 (1997) 6548–6558.
[38] E. Blanc, P. Roversi, C. Vonrhein, C. Flensburg, S.M. Lea, G. Bricogne, Refinement of severely incomplete structures with maximum likelihood in BUSTER-

TNT, Acta Crystallogr. D. Biol. Crystallogr. 60 (2004) 2210–2221.
[39] P. Emsley, K. Cowtan, Coot: model-building tools for molecular graphics, Acta Crystallogr. D. Biol. Crystallogr. 60 (2004) 2126–2132.
[40] S.G. Rogers, B. Weiss, Exonuclease III of *Escherichia coli* K-12, an AP endonuclease, Methods Enzymol. 65 (1980) 201–211.
[41] P. Prorok, D. Alili, C. Saint-Pierre, D. Gasparutto, D.O. Zharkov, A.A. Ishchenko, B. Tudek, M.K. Saparbaev, Uracil in duplex DNA is a substrate for the nucleotide incision repair pathway in human cells, Proc. Natl. Acad. Sci. U. S. A. 110 (2013) E3695–E3703.
[42] P. Prorok, C. Saint-Pierre, D. Gasparutto, O.S. Fedorova, A.A. Ishchenko, H. Leh, M. Buckle, B. Tudek, M. Saparbaev, Highly mutagenic exocyclic DNA adducts are substrates for the human nucleotide incision repair pathway, PLoS One 7 (2012) e51776.
[43] P. Retailleau, A.A. Ishchenko, N.A. Kuznetsov, M. Saparbaev, S. Morera, Crystallization and preliminary X-ray analysis of human endonuclease 1 (APE1) in complex with an oligonucleotide containing a 5,6-dihydrouracil (DHU) or an alpha-anomeric 2'-deoxyadenosine (alphadA) modified base, Acta Crystallogr. Sect. F. Struct. Biol. Cryst. Commun. 66 (2010) 798–800.
[44] B.A. Manvilla, E. Pozharski, E.A. Toth, A.C. Drohat, Structure of human apurinic/apyrimidinic endonuclease 1 with the essential Mg2+ cofactor, Acta Crystallogr. D. Biol. Crystallogr. 69 (2013) 2555–2562.
[45] D.R. McNeill, A. Narayana, H.K. Wong, D.M. Wilson 3rd, Inhibition of Ape1 nuclease activity by lead, iron, and cadmium, Environ. Health Perspect. 112 (2004) 799–804.
[46] E. Krissinel, K. Henrick, Secondary-structure matching (SSM), a new tool for fast protein structure alignment in three dimensions, Acta Crystallogr. D. Biol. Crystallogr. 60 (2004) 2256–2268.
[47] L.F. Melo, S.T. Mundle, M.H. Fattal, N.E. O'Regan, P.R. Strauss, Role of active site tyrosines in dynamic aspects of DNA binding by AP endonuclease, DNA Repair (Amst) 6 (2007) 374–382.
[48] A.A. Ishchenko, X. Yang, D. Ramotar, M. Saparbaev, The 3'->5' exonuclease of Apn1 provides an alternative pathway to repair 7,8-Dihydro-8-Oxodeoxyguanosine in Saccharomyces cerevisiae, Mol. Cell. Biol. 25 (2005) 6380–6390.
[49] J.A. Lucas, Y. Masuda, R.A. Bennett, N.S. Strauss, P.R. Strauss, Single-turnover analysis of mutant human apurinic/apyrimidinic endonuclease, Biochemistry 38 (1999) 4958–4964.
[50] R. Moeller, M. Raguse, G. Reitz, R. Okayasu, Z. Li, S. Klein, P. Setlow, W.L. Nicholson, Resistance of Bacillus subtilis spore DNA to lethal ionizing radiation damage relies primarily on spore core components and DNA repair, with minor effects of oxygen radical detoxification, Appl. Environ. Microbiol. 80 (2014) 104–109.
[51] G. Golan, A.A. Ishchenko, B. Khassenov, G. Shoham, M.K. Saparbaev, Coupling of the nucleotide incision and 3'–>5' exonuclease activities in Escherichia coli endonuclease IV: structural and genetic evidences, Mutat. Res. 685 (2010) 70–79.
[52] J.P. Erzberger, D.M. Wilson 3rd, The role of Mg2+ and specific amino acid residues in the catalytic reaction of the major human abasic endonuclease: new insights from EDTA-resistant incision of acyclic abasic site analogs and site-directed mutagenesis, J. Mol. Biol. 290 (1999) 447–457.
[53] R.L. Maher, L.B. Bloom, Pre-steady-state kinetic characterization of the AP endonuclease activity of human AP endonuclease 1, J. Biol. Chem. 282 (2007) 30577–30585.
[54] T. Izumi, J. Malecki, M.A. Chaudhry, M. Weinfeld, J.H. Hill, J.C. Lee, S. Mitra, Intragenic suppression of an active site mutation in the human apurinic/apyrimidinic endonuclease, J. Mol. Biol. 287 (1999) 47–57.
[55] N. Oezguen, C.H. Schein, S.R. Peddi, T.D. Power, T. Izumi, W. Braun, A "moving metal mechanism" for substrate cleavage by the DNA repair endonuclease APE-1, Proteins 68 (2007) 313–323.
[56] D. Fantini, C. Vascotto, D. Marasco, C. D'Ambrosio, M. Romanello, L. Vitagliano, C. Pedone, M. Poletto, L. Cesaratto, F. Quadrifoglio, A. Scaloni, J.P. Radicella, G. Tell, Critical lysine residues within the overlooked N-terminal domain of human APE1 regulate its biological functions, Nucleic Acids Res. 38 (2010) 8239–8256.
[57] G. Antoniali, L. Lirussi, C. D'Ambrosio, F. Dal Piaz, C. Vascotto, E. Casarano, D. Marasco, A. Scaloni, F. Fogolari, G. Tell, SIRT1 gene expression upon genotoxic damage is regulated by APE1 through nCaRE-promoter elements, Mol. Biol. Cell 25 (2014) 532–547.
[58] L. Lirussi, G. Antoniali, C. Vascotto, C. D'Ambrosio, M. Poletto, M. Romanello, D. Marasco, M. Leone, F. Quadrifoglio, K.K. Bhakat, A. Scaloni, G. Tell, Nucleolar accumulation of APE1 depends on charged lysine residues that undergo acetylation upon genotoxic stress and modulate its BER activity in cells, Mol. Biol. Cell 23 (2012) 4079–4096.
[59] D. Lu, J. Silhan, J.T. MacDonald, E.P. Carpenter, K. Jensen, C.M. Tang, G.S. Baldwin, P.S. Freemont, Structural basis for the recognition and cleavage of abasic DNA in Neisseria meningitidis, Proc. Natl. Acad. Sci. U. S. A. 109 (2012) 16852–16857.